PHYSICAL CHEMISTRY OF SLAGS PRODUCED IN THE PROCESSING OF NON-FERROUS METALS

J.M. Toguri

Department of Metallurgy
and Materials Science
University of Toronto
Toronto, Ontario
CANADA M5S 1A4

Synopsis

Recent advances in our understanding of non-ferrous slags in contact with either matte or metal phase will be discussed form the perspective of impurity distribution and pay metal losses. The migratory behaviour of matte droplets in slag shows specific directionality when subjected to an external electric field due to the electrocapillary motion of the droplets. It is found that the migration direction depends on matte and slag composition. The role of interfacial phenomena between slags and matte/metal and its effect of the entrainment loss of the respective pay metal are discussed.

Introduction

In the pyrometallurgical production of non-ferrous metals, such as copper and nickel, the slag acts as a collector for iron and gangue materials in the feed and also provides one of the means for elimination of the various minor elements. Much attention has been given to studies of minor element deportment in copper smelting systems (1-6).

Distribution Ratio Copper-Slag

The distribution ratio of an element X between liquid copper and slag is defined as $L_X^{C/S} = [\%X]/(\%X)$ where [%X] and (%X) are the weight percent of an element X in copper and slag, respectively. The distribution of most minor elements between copper and slag is almost independent of the type of slag used but very dependent on the oxygen pressure. The distribution ratios of several minor elements between liquid copper and iron silicate slag at 1523K (1,3,7) are shown in Fig. 1. The order of the tendency to concentrate in the copper phase is as follows: Ag>Sb>As>Cu>Ni>Sn>Pb>Co>Zn>Fe>Mo.

The distribution ratio for several elements between liquid copper and calcium ferrite slag at 1250°C is shown in Fig.2. The distribution behaviour is quite similar to that for the iron silicate slag. The distribution ratios for Fe, Co, Ni, Cu and Bi are essentially the same for the two types of slag. The distribution ratios of Zn and Pb are much larger in the ferrite slag than in the silicate slag. Thus silicate slags are more effective than ferrite slags for removal of Zn and Pb from liquid copper. The dissolution ratios for Sn, As and Sb are much larger for the silicate slag. Thus, ferrite slags are more convenient for oxidative removal of these elements from copper. The basic ferrite slag is convenient to fix the acidic oxides. However, the high distribution ratios of As, Sb and Bi, suggest that the removal of these elements from liquid copper is not very easy.

Distribution Ratio Matte-Slag

The distribution of an element X between matte and slag is defined as follows: $L_X^{m/s} = [\%X]/(\%X)$ where [%X] and (%X) are the weight percent of the element in the matte and slag, respectively. Figure 3 shows the distribution ratios between matte and slag (1,3) as a function of oxygen pressure for several elements under coexistence with a liquid copper phase. The distribution ratios under oxidizing conditions (P_{SO_2} = 0.1 atm) are plotted in Fig. 4 as a function of the matte grade. Data by Sinha and Nagamori (8) are also presented in the same figure. The two sets of results seem to fit well with each other, even though the experiments by Sinha and Nagamori were carried out under copper saturation. The trend for all elements is to enter the slag phase at higher matte grades with the exception of As.

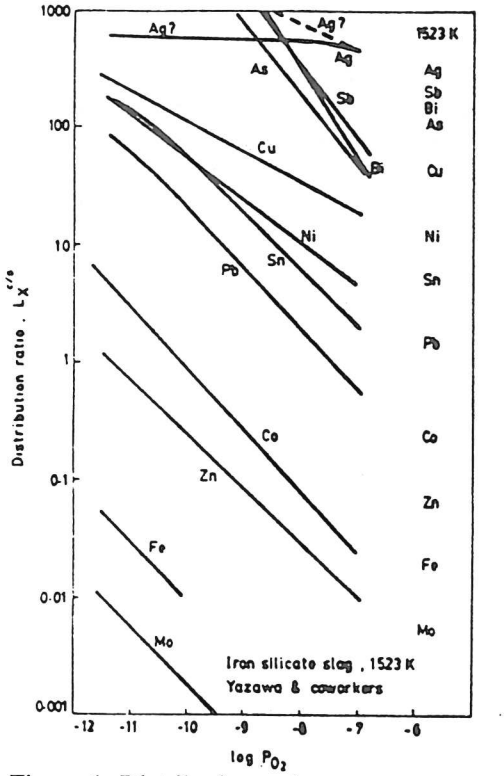

Figure 1. Distribution ratios, liquid copper-iron silicate slag.

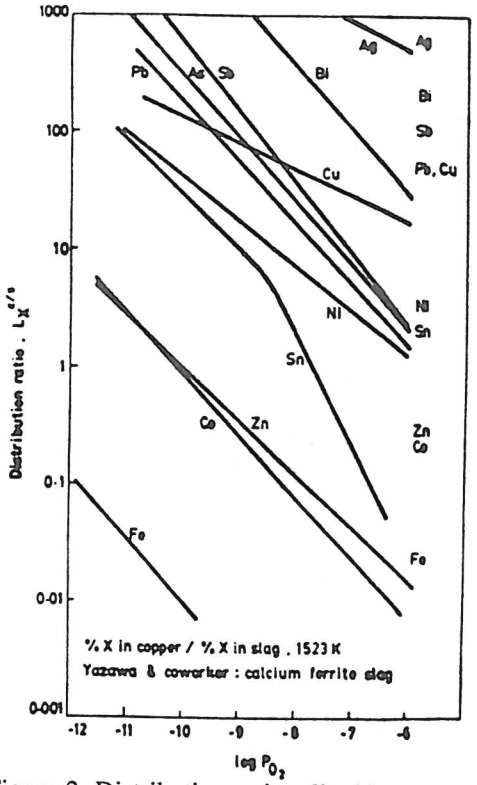

Figure 2. Distribution ratios, liquid copper-calcium ferrite slag at 1250°C.

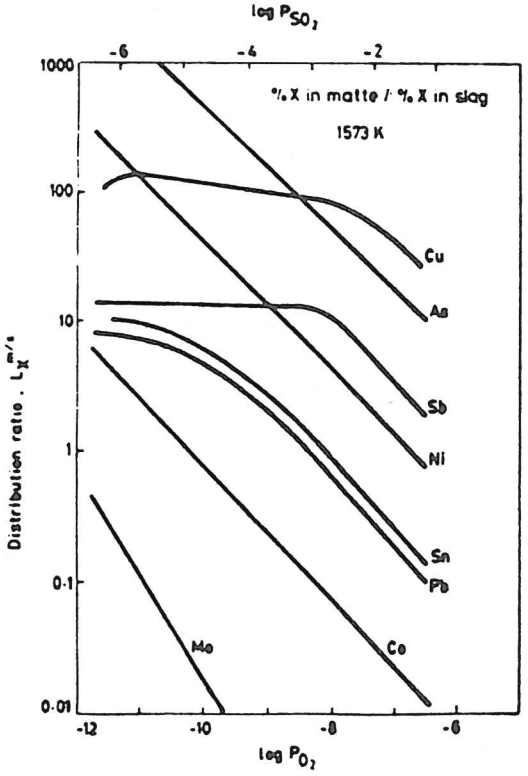

Figure 3. Distribution ratios for several elements between matte and slag at 1573K (1,3).(coexistence of liquid copper).

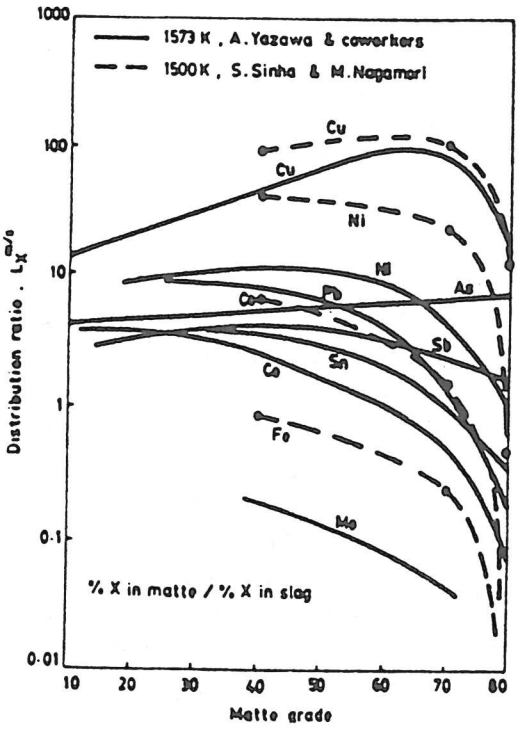

Figure 4. Distribution ratios for various elements between matte and slag plotted against the matte grade.

Nickel Matte-Slag System

The distribution equilibria of several minor elements in the nickel matte-slag system at 1523 have been reported by Celmer and Toguri (9,10). Minor element distribution relationships for the oxidizing smelting region (P_{SO_2} = 0.1 or 0.01 bar) are summarized in Fig. 5 for the case of Ni matte and additive-free slag.

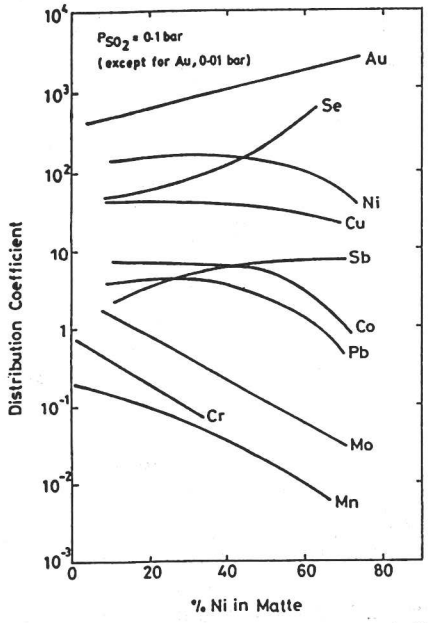

Figure 5. Minor element and nickel distributions nickel matte and silica-saturated iron silicate slag at 1523K.

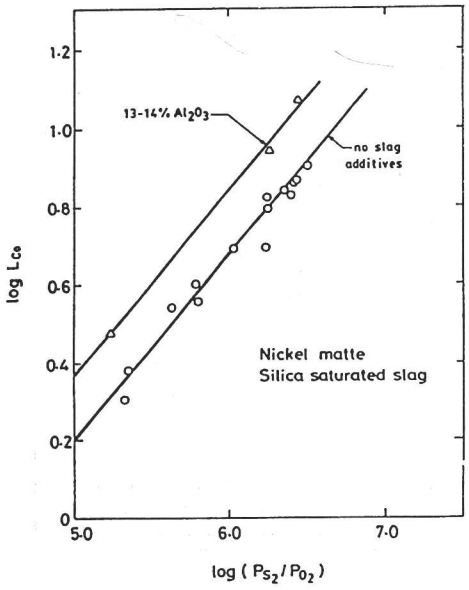

Figure 6. Variation of the cobalt distribution coefficient with gas potential ratio, under 0.1 bar SO_2.

Modelling of the Distribution Equilibria

Cobalt dissolution into slags (11) has been identified as an oxidative process by Wang et al. (12,13) for alloy-slag systems and by Yazawa (1) for matte-copper-slag systems. Under oxidative and smelting conditions, the equilibrium between cobalt in matte and slag may be given by equation [1]:

$$\{CoS\} + \tfrac{1}{2}\, O_2 = (CoO) + \tfrac{1}{2}\, S_2 \qquad [1]$$

Plots of the distribution coefficients for cobalt against the sulphur-oxygen potential ratio, shown in Fig. 6, support this mechanism. For silica-saturated slag with no additives, $\log L_{Co}^{m/s} = 0.4744 \log (P_{S_2}/P_{O_2}) - 2.172$ For silica-saturated slag containing 15% Al_2O_3, $\log L_{Co}^{m/s} = 0.4716 \log (P_{S_2}/P_{O_2}) - 1.988$ In the dilute solution regime, the distribution coefficient is expressed by,

$$L_{Co}^{m/s} = \frac{\gamma^{\circ}_{CoO}}{\gamma^{\circ}_{CoS}} \frac{1}{K_{(1)}} K'' \frac{P_{S_2}^{0.5}}{P_{O_2}} \qquad [2]$$

where $K_{(1)}$ is the equilibrium constant for reaction [1]. The linear relationship of Fig. 6, with exponent close to 0.5, demonstrates the near constancy of the ratio of activity coefficients of cobalt species. Cobalt partition may also be expressed in terms of condensed phase variables by use of the exchange reaction:

$$\{CoS\}(\ell) + (FeO)(\ell) = (CoO)(\ell) + \{FeS\}(\ell) \qquad \Delta G^{\circ}_{(5)} = 34978 - 8.87\ T\ J\ mol^{-1} \qquad [3]$$

$$L_{Co}^{m/s} = \frac{a_{FeS}}{a_{FeO}} \frac{\gamma^{\circ}_{CoO}}{\gamma^{\circ}_{CoS}} \frac{n_{T_m}}{n_{T_s}} \frac{1}{K_{(3)}} \qquad [4]$$

where n_T = molar quantity of matte and slag constituents in the $NiS_{0.67}$, FeS, CoS, CoO, FeO, $FeO_{1.33}$, SiO_2 system; average values determined by chemical analyses of the phases were n_{T_m} = 1.21 and n_{T_s} - 1.48. The activity of FeS in oxygen-containing Ni matte was evaluated from the iron sulphide-oxide equilibrium:

$$FeS(\ell) + \tfrac{1}{2} O_2 (g) = FeO (\ell) + \tfrac{1}{2} S_2 (g) \quad [5]$$

Taking free energy data from Mackey (14), and a_{FeO} = 0.35 for silica-saturated slag then

$$a_{FeS} = 1.78 \times 10^{-4} \ (P_{S_2}/P_{O_2})^{0.5} \quad [6]$$

Cobalt distributions are shown for the Ni smelting system in Fig. 7, as a function of a_{FeS} computed by equation [6]. Also given are the data for Cu-Ni matte (9:1), with a_{FeS} from reported copper smelting studies (15). The value of γ_{CoO} was computed from the solubility measurements of Wang et al. (12,13), giving $\gamma_{CoO}(\ell)$ = 0.79. Similarly, γ_{CoS} = 0.40 was abstracted from the work of Sinha and Nagamori (8) for FeS-CoS-Cu_2S mattes. The distribution coefficients calculated by equation [4] are presented in Fig. 8. Results given in Figs. 7 and 8 show that cobalt distributions are strongly sensitive to two important thermodynamic variables in smelting - sulphur and oxygen potentials. With increasing matte grade, or decreasing (P_{S_2}/P_{O_2}) ratio, Co recovery to matte falls rapidly. At matte grades greater than 65% Ni, Co distributes preferentially into the slag phase. In smelting practice, high Co recoveries can only be achieved under reducing conditions.

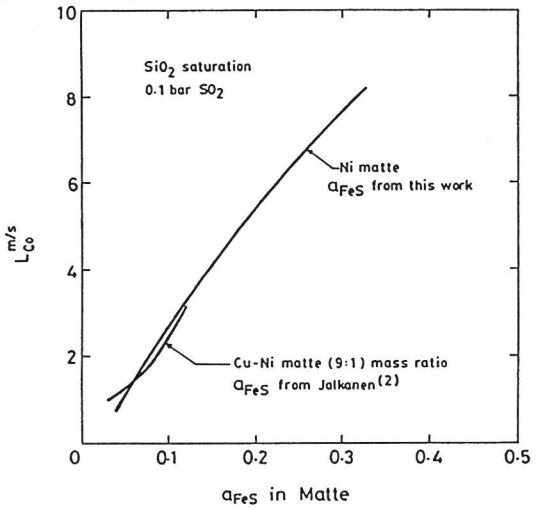

Figure 7. Cobalt distributions as a function of the FeS activity in matte.

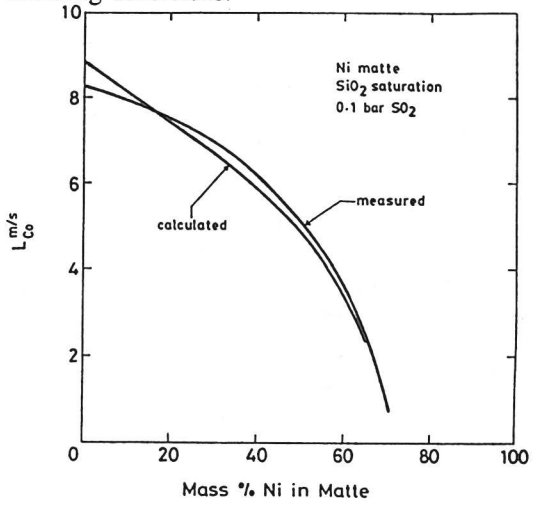

Figure 8. Comparison of calculated cobalt distribution with experimental results.

Electrodynamic Behaviour of Metal and Metal Sulphide Droplets in Slags

Recently, the governing physiochemical hydrodynamic equations describing the behaviour of a liquid droplet under the influence of an electric field was discussed (16). The movement of a second liquid phase, such as molten droplets of pay metal or metal sulphides, in a liquid electrolyte, such as slag, is referred to as electrocapillarity. The migration of these droplets is due to the interaction between the electric field and the interfacial tension of the drop. The study of electrocapillarity has been carried out quite extensively in the Soviet Union. The application of electrocapillarity to assist in the settling process and thus enhance the recovery of pay metal appears as a promising mode of slag cleaning.

A very simplistic and conceptual description of the motion of a metal droplet in solution when subjected to an external electric field has been given by Christiansen (17). Consider firstly a metal droplet which is ideally polarized in solution. A double layer is formed and the charges are randomly distributed as shown in Fig. 9(a). If an external electric field is applied which is directed to the right (Fig. 9(b)), there will be a re-orientation of charges such that there are more positive charges on the right and less on the left side of the droplet. This imbalance of charges at the left and right sides of the droplet will cause these regions to have different interfacial tensions. If the left side has a lower interfacial tension than the right, then fluid motion will be induced along the circumference of the drop due to the interfacial tension gradient. The surface fluid will flow from a region of low to a region of high interfacial tension in order to minimize surface energy. This surface motion of the droplet will also drag adjacent layers of electrolyte. As a result, the entire droplet moves to the left along lines of constant current due to the shear forces between the droplet and the electrolyte.

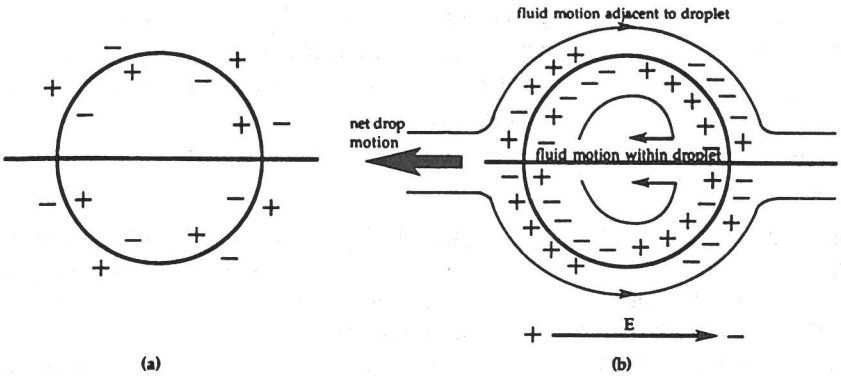

Figure 9. Charge distribution of droplet (a) in solution and (b) under the influence of an electric field, E. In (a), the charges are randomly distributed while in (b), the charges are polarized about the equator as a result of the external electric field.

ELECTRODYNAMIC EQUATION

The formulation of the mathematical statements describing the flow shown in Fig. 9(b) had been reported by Levich (18). In a recent study, we have followed Levich's approach to model the electrodynamic behaviour of sulphide droplets in slags (16). The analyses consisted of statements describing conservation of electric charges due to the applied electric field, conservation of surface species at the interface, and conservation of mass and momentum for the droplet and surrounding media. The equation for the migration rate of an ideally polarized droplet in a conducting media is:

$$U = \varepsilon Ea/2\mu + 3\mu' + (\varepsilon^2/X) \qquad [7]$$

where E = applied electric field (V/m), a = droplet radius (m), μ = electrolyte viscosity, μ' = droplet viscosity (kg/m-s), X = electrical conductivity of electrolyte ($\Omega^{-1}m^{-1}$) and ε = surface charge density (C/m^2). ε is obtained from the slope of the electrocapillary diagram (Fig. 10) which is a plot of the interfacial tension versus the potential drop across the interface.

Mechanism for Droplet Migration Directionality

The electrocapillary maximum (ecm) is usually on one side of the diagram. Under the above condition, three motions can be induced onto the droplet (Fig. 11(a)): net left motion, net right motion, and no net motion. Note that the slope on the left and right arms of the electrocapillary diagram (Fig. 11(b)) are not the same. This asymmetry is suggested to be the principal factor controlling the droplet's migration rate and direction.

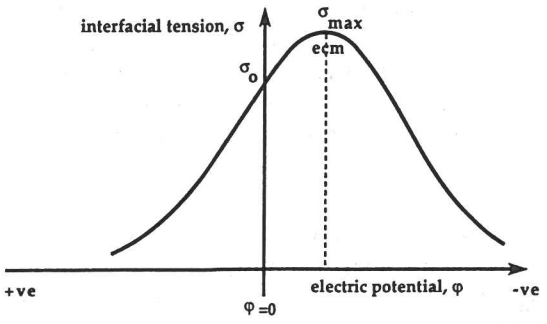

Figure 10. Electrocapillary diagram σ_0 is the interfacial tension when no voltage is applied. σ_{max} is the electrocapillary maximum (ecm).

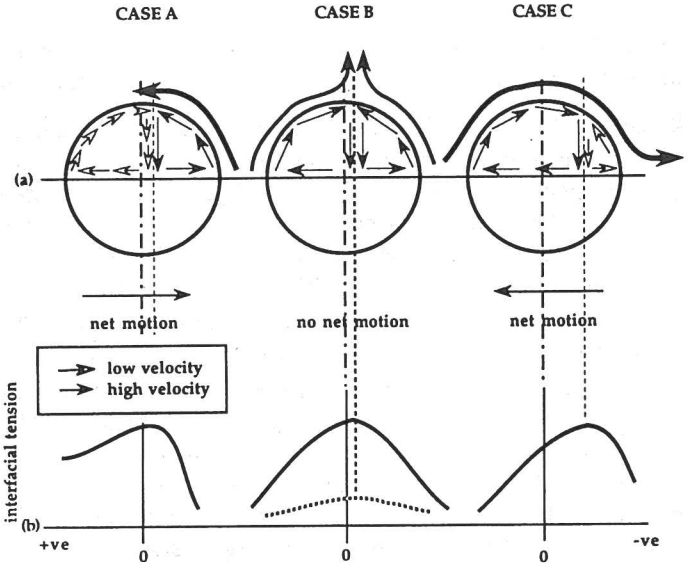

Figure 11. a) Possible electrocapillary motion due to b) electrocapillary curves with a single maxima. Case A -net right motion: Case B - no motion: Case C - net left motion.

When faradaic processes occur at the interface, the droplet is said to be partially polarized and eqn. [7] is modified as (18):

$$U_{pp} = \varepsilon\, Ea/\,(2\mu + 3\mu')\,(1 + \frac{a}{2X\omega}) + \frac{\varepsilon^2}{X}$$

where ω, the interfacial resistance, defined by: $\omega = RT/zFi_{lim}$ is a measure of the partial polarization at the interface. i_{lim} is the limiting current density at the interface due to ion transport by diffusion.

Analyses of Electrocapillary Motion of Droplets in Slag

The experimental observation of the migration rates and directions of Cu2S-FeS matte droplets in FeO-CaO-Al2O3-SiO2 slag system was discussed in a previous publication (16). The electrocapillary motions of these liquid droplets were observed on the surface of a horizontal boat in 50% Ar-CO reducing atmosphere at 1250 °C. An electric field was created through two Mo electrodes dipped at each end of the alumina boat.

Figure 12 shows the migration rate and direction of various droplets in synthetic fayalite at 1250 °C while Fig. 13 shows the migration velocity of Cu2S in similar slags under similar conditions but as a function of electric field and droplet radius. The positive velocity indicates migration to the anode. The migration equation (eqn. [7]) can be qualitatively verified for the cases studied in Figs. 12-13. The migration rate increases as the droplet size or applied potential field is increased. Figure 12 is particularly interesting as it shows that the droplets can migrate to either electrode. When a Cu2S droplet was placed near the cathode and an FeS droplet placed near the anode, it was seen that the droplets migrate to the opposite electrodes when the electric field was applied. In fact, the droplets migrated past each other across the surface of the slag. Such independent motions suggest the possibility of specific control of the droplet's migration behaviour which can be advantageous during slag cleaning operation.

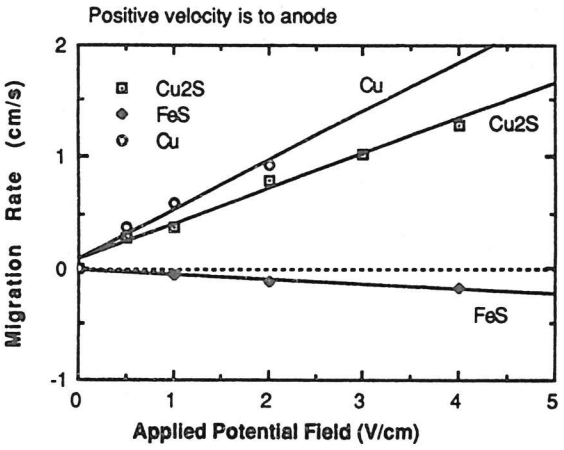

Figure 12. Migration rates of copper, copper sulphide, and iron sulphide droplets on the surface of synthetic fayalite slag (70% FeO) versus applied potential field at 1250°C (50% Ar-CO).

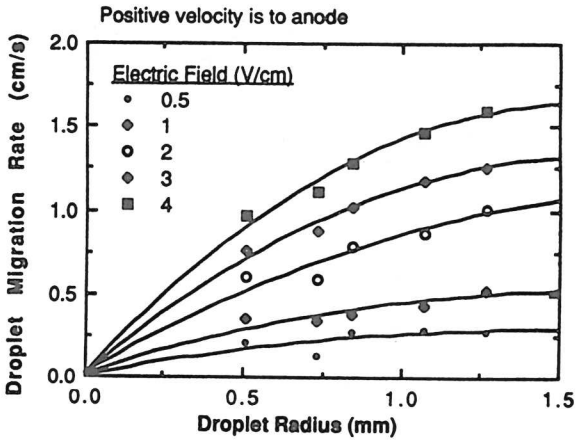

Figure 13. Migration rates of copper sulphide droplets on the surface of synthetic fayalite slag (70% FeO) as a function of drop radius for various potential fields at 1250°C (50% Ar-CO). The values shown on the figure refer to the electric field strength.

Figure 13 shows parabolic-type relationship rather than the linear function expressed in eqn. [7]. This observation can be attributed to partial polarization as described via eqn. [8]. Partial polarization occurs when there is ion exchange or charge transfer at the droplet-electrolyte interface. Thus, i_{lim} is non-zero and U_{pp} (eqn. [8]) is depressed with respect to U_p (eqn. [7]).

In the case of a metal-slag or a metal sulphide-slag system , the following assumptions can be applied to eqn. [8]: i) the droplet viscosity is much lower than the slag viscosity: $\mu' << \mu$; ii) the electrolyte has high viscosity and electrical conductivity but low surface charge: $2\mu + 3\mu' >> \varepsilon^2/\chi$.

Under these conditions, eqn. [8] is reduced to :

$$\underline{U}_{pp} = \varepsilon Ea/2\mu(1 + (a/2X\omega)) \quad [9]$$

Equation [9] can be used to obtain an order of magnitude of the interfacial tension, ω, and the surface charge density, ε. From the least square analysis of Fig. 14 via eqn. [13], the following values can be derived for Cu2S matte droplets (a=0.51 mm to 1.27 mm) in synthetic fayalite under 50%Ar-CO atmosphere at 1250 °C:

$$\varepsilon = (1.3\pm0.3)x10^{-2}C/m^2;\ \omega = (0.7\pm0.2)x10^{-5}\Omega m^2;\ k = 1.8\pm0.3;\ i_{lim} = (0.9\pm0.2)x10^4 A/m^2 \quad [10]$$

These represent the average values for the system examined. The largest uncertainty of these results is at most 30%.

Prior to our study, Kammel (19) and Chlipov and Esin (20) had also examined the role of FeO in slag. Kammel examined the electrocapillary behaviour of Cu_2S, Ni_3S_2, and PbS in a $CaO\text{-}Al_2O_3\text{-}SiO_2$ slag both in the presence and absence of FeO. Our results for Cu_2S-FeS droplets in $FeO\text{-}CaO\text{-}Al_2O_3\text{-}SiO_2$ under reducing atmosphere are shown in Figs. 14-15. In general, the results of all studies are consistent: for example, all studies found that virgin metal sulphide (Cu_2S, Ni_3S_2, and PbS) migrates to the anode in FeO-free slag.

Figures 14 and 15 show that as one species is progressively reduced to zero, the droplet behaviour can change dramatically. For instance, the absence of Cu in the FeS droplet (Fig. 14) resulted in the mobility having a maxima while the rest of the Cu_2S-FeS droplets' mobilities have minima. Similarly, the absence of FeO in the slag (Fig. 15) produces only positive mobilities with increasing Cu content in mate while the presence of FeO can create both positive and negative mobilities. The obvious explanation for both positive and negative mobilities is due to the shift in the electrocapillary curves with composition. Furthermore, the slope of these curves should indicate the type of charges (positive or negative) present at the interfacial region, and from which the redox reactions can be predicted. Thus, the determination of the electrocapillary diagram is an important and most logical step of this investigation. This work is presently in progress in our laboratory.

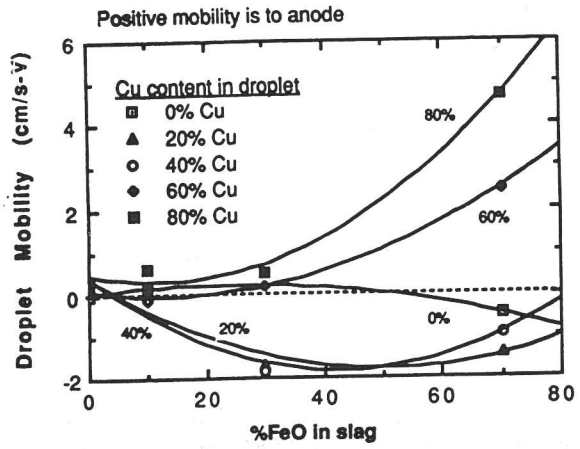

Figure 14. Mobility of Cu_2S-FeS as a function of FeO content in slag (1300°C: 50% Ar-CO). Mobility = (migration rate)/(applied potential field · droplet radius) = U/Ea.

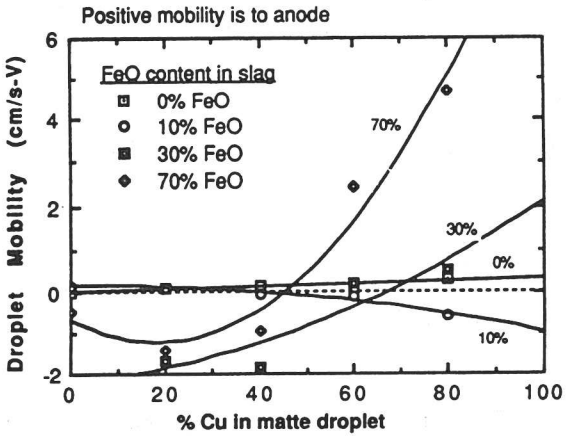

Figure 15. Mobility of Cu_2S-FeS as a function of Cu content in matte droplet (1300°C: 50% Ar-CO).

Acknowledgements

The author thanks the Natural Sciences and Engineering Research Council of Canada for financial support of this investigation. Without the assistance of the numerous graduate students, particularly Dr. R. Celmer and Dr. R.T.C. Choo, the present studies would not have been possible.

References

(1) A. Yazawa, "Extractive Metallurgical Chemistry with Special Reference to Copper Smelting," Paper presented at the 28th Congress of IUPAC, Vancouver, B.C., Canada, Aug. 1981.
(2) A. Yazawa, S. Nakazawa, Y. Takeda, "Distribution Behaviour of Various Elements in Copper Smelting Systems," in Advances in Sulfide Smelting, Vol. 1, H.Y. Sohn, D.B. George, A.D. Zunkel (eds.), TMS AIME, 1983, pp. 99-117.
(3) G.H. Kaiura, K. Watanabe, A. Yazawa, Can. Metall. Q., Vol. 19, 1980, pp. 191-200.
(4) E.A. Johnson, P.E. Sanker, L.L. Oden, J.B. See, U.S. Bureau of Mines Report of Investigations 8655, United States Dept. of the Interior, 1982.
(5) H.K. Jalkanen, L.E.K. Holappa, J.K. Makinen, "Some Novel Aspects of Matte-Slag Equilibria in Copper Smelting," in Advances in Sulfide Smelting, Vol. 1 H.Y. Sohn, D.B. George, A.D. Zunkel (eds.), TMS AIME, 1983, pp. 277-292.
(6) Y. Takeda, S. Ishiwata, A. Yazawa, Trans. JIM, 24, 518(1983).
(7) M. Kashima, M. Eguchi, A. Yazawa, ibid., 19, 152(1978).
(8) S.N. Sinha, M. Nagamori, Met. Trans. B, 13B, 461(1982).
(9) R.S. Celmer, J.M. Toguri, Proceedings Nickel Metallurgy, Vol. 1, 1986 CIMM, pp. 165-183.
(10) R.S. Celmer, J.M. Toguri, Proceedings of the Terkel Rosenquist Symposium, Norwegian Inst. Tech., 1988, pp. 341-368.
(11) J. Matousek, "The Pyrometallurgical Winning of Cobalt," Paper presented at The Canadian Institute of Mining and Metallurgy, Annual General Meeting, Calgary, Alberta, May 4-6, 1981.
(12) S.S. Wang, N.H. Santander, J.M. Toguri, Metall. Trans., Vol. 5, 1974, pp. 261-265.
(13) S.S. Wang, A.J. Kurtis, J.M. Toguri, Can. Metall. Q., Vol. 12, 1973, pp. 383-390.
(14) P.J. Mackey, Can. Metall. Q., Vol. 21, 1982, pp. 221-260.
(15) T. Rosenqvist, "Thermodynamics of Copper Smelting," in Advances in Sulfide Smelting, Vol. 1, H.Y. Sohn, D.B. George, A.D. Zunkel (eds.), TMS AIME, 1983, pp. 239-255.
(16) R.T.C. Choo, J.M. Toguri - Can. Met. Q., Vol. 31, 1992, pp. 113-126.
(17) S. Christiansen, Ann. Phys., 12 No. 4 (1903), 1072.
(18) V.G. Levich, Physiochemical Hydrodynamics, Prentice-Hall, Englewood Cliffs (1962), pp. 472-531.
(19) R. Kammel, Eerzmetall, 27 No. 3 (1974), 135-143.
(20) V.V. Chlipov, O.A. Esin, Doklady AN SSSR, 123 No. 2 (1958), 320-323.